Journal of Applied Physics

Analysis of a nonorthogonal pattern of misfit dislocation arrays in SiGe epitaxy on high-index Si substrates

Cite as: Journal of Applied Physics **95**, 115 (2004); https://doi.org/10.1063/1.1630362
Submitted: 15 August 2003 • Accepted: 07 October 2003 • Published Online: 16 December 2003

Morgan E. Ware, Robert J. Nemanich, Jennifer L. Gray, et al.

JOURNAL OF APPLIED PHYSICS VOLUME 95, NUMBER 1 1 JANUARY 2004

Analysis of a nonorthogonal pattern of misfit dislocation arrays in SiGe epitaxy on high-index Si substrates

Morgan E. Ware and Robert J. Nemanich[a)]
Department of Physics, North Carolina State University, Raleigh, North Carolina 27695-8202

Jennifer L. Gray and Robert Hull
Department of Material Science and Engineering, University of Virginia, Charlottesville, Virginia 22904

(Received 15 August 2003; accepted 7 October 2003)

We have investigated the formation of misfit dislocations resulting from the growth of partially strained $Si_{0.7}Ge_{0.3}$ epitaxial films on Si substrates with surface normals rotated off of the [001] axis toward [110] by 0°, 13°, and 25°. Transmission electron microscopy has shown that the dislocations form in a modified cross-hatch pattern for samples grown on the off-axis substrates. This modified cross hatch consists of three arrays along which the dislocations align. This is in contrast to the two orthogonal arrays found on the on-axis (001) substrates. These dislocations correspond well with the intersection of the (111) slip planes with the respective surfaces. We present a simple analysis of the amount of relaxation due to probable Burger's vectors for these dislocations, which reveals the most likely directions for these vectors and shows that the density of dislocations only accounts for a fraction of the total film relaxation as measured by Raman peak shifts. These studies form the basis for the use of high index surfaces as components in modern devices, and provide pathways to possible templates for use in the growth of nanostructures.
[DOI: 10.1063/1.1630362]

I. INTRODUCTION

The low-index surfaces of silicon are well understood,[1] and technological applications of SiGe epitaxy on those substrates, mainly (001), are starting to become commercially available.[2] Recent developments, though, in the understanding of a large class of high-index Si surfaces[3–5] have paved the way for the study of SiGe epitaxy on those surfaces. These are the surfaces with normals lying in the plane containing and between the [001] and [111] directions. Throughout this article, these surfaces will be referenced by an angle of rotation, θ, of the surface normal from the [001] axis toward the [111] direction. Distinguishing this family are surface features, either atomic steps or facets, which are aligned in the $[1\bar{1}0]$ direction. These features are summarized in Table I. Relatively little is known about SiGe epitaxy on most of these surfaces or the effect of the steps and facets on growth.

Si surfaces with small deviations from the low-index surfaces have been used in a limited number of studies of SiGe epitaxy.[6–12] Lapena and co-workers[6] have grown SiGe on Si surfaces up to 10° off (111) toward (001), i.e., θ=44.7°–54.7° in our notation. They have found the surface morphology to be characterized by large-scale coherent undulations which vary with the substrate orientation. Berbezier and co-workers[7] investigated the surface morphology of samples up to 10° in our notation and also found unique surface structures similarly characterized by varying surface ripples. Both groups used coherently strained samples that were grown below the critical thickness for dislocation formation and therefore are not influenced by the inclusion of dislocations. Our studies of strain relaxed samples have shown that surface undulations similar to those found by others on strained films[6,7] tend to be organized on the surface of a relaxed film and, along the same lines, the misfit dislocations follow at the film–substrate interface.[8]

The (113) surface at 25.2° has also been studied and is exceptional in that stable reconstructions have been known to form on this surface of Si for many years.[9] Several groups have examined Ge and SiGe growth on the (113) surface. A 5–8 monolayer film of Ge on this surface of Si grown between 400 °C and 500 °C produces nanowires in the $[33\bar{2}]$ direction which are about 20 nm wide by 150 nm long with facetted sides.[10] Notably, two groups have investigated the growth of Ge on SiGe multilayers grown on Si (113) substrates.[11,12] They found that the multilayers helped form more uniform wires or dots in some cases, and aided in their organization. An aspect that has not been extensively studied though, is the process by which SiGe layers grown on these high-index surfaces relax plastically due to dislocation formation.

Comprehensive reviews on misfit dislocations in low-index systems are given by van der Merwe[13] and Hull and Bean.[14] As they explain, lattice mismatched epitaxy has classically been characterized by a critical thickness, i.e., that thickness above which it is energetically favorable to form misfit dislocations to relax the strain in the layer.[15] The SiGe/Si heteroepitaxial system is well suited to study lattice mismatched epitaxy and the concept of critical thickness. This is mainly because Si processing, which is extendable to SiGe, is so well developed due to the semiconductor industry that imperfections in the substrates and the growth can, in

[a)]Electronic mail: robert_nemanich@ncsu.edu

TABLE I. Summary of the family of surfaces between (001) and (111) and their major surface features. The A subscript indicates that the dimerization axis of the higher terrace is perpendicular to the step edge and the B subscript that the dimerization axis is parallel to the step edge.

Surface: (hkl) or $\{\theta\}$	Terraces	Step or facet structure	Reference No.
(001) to ∼1°	(001) 2×1 terraces	Steps: Single, S_A and S_B	4, 5
∼1° to ∼6°	(001) 2×1 terraces	Steps: S_A, S_B, double D_B (rebonded)	3
∼6° to ∼11°	(001) 2×1 terraces Single domain	Steps: D_B (rebonded)	3
∼11° to (116) {13.3°}	(001) 2×1 terraces Single domain	Steps: D_B rebonded and nonrebonded	3
(116) to (114)	(001) and (114)	Steps: D_B rebonded and nonrebonded	3
(114) {19.5°}	(114) tetramers		3
(114) to (113)	(114) and (113)	Facets: Saw tooth mesoscale	3
(113) {25.2°}	(113) 3×2		3
(113) to (5,5,12)	(113) and (7,7,17)	Facets: Saw tooth mesoscale	3
(5,5,12) {30.5°}	(5,5,12) 2×1 terraces		3
(5,5,12) to ∼43°	(5,5,12) and (111)	Facets: Nanoscale	3
∼43° to (111) {54.7°}	(111) 7×7 terraces	Steps: Single and triple	3

many cases, be excluded from consideration. This system can also exhibit a relatively wide range of mismatch by varying the Ge concentration which is useful in studying lattice mismatched epitaxy. This mismatch, defined as the strain, ϵ, in a coherent layer of $Si_{1-x}Ge_x$ can be shown to be proportional to the Ge concentration, x, at room temperature as[16]

$$\epsilon(x) = 0.0409x. \tag{1}$$

Accordingly, upon growth to the critical thickness, dislocations are predicted to form[17] and glide along slip planes which are known in the diamond lattice to be the {111} planes.[16] Following this initial relaxation step are several stages of dislocation motion, multiplication, and interaction which are all kinetically driven and are only recently being explored theoretically and experimentally.[16,18,19] In this article, we will focus our discussion, though, on static characteristics of the dislocations.

As shown in Fig. 1, there are four {111} planes which intersect this family of surfaces. On the (001) surface, $\theta = 0$, two {111} planes each intersect along the [110] and [110] directions. As the surface is rotated off axis, i.e., $\theta > 0$, the two planes which intersected along [110] begin to split in the plane of the surface. Specifically, the lines of intersection of the (111) and (111) planes with the surface now intersect at an angle, φ, given by

$$\cos(\phi) = \frac{2 + \tan(\theta)^2}{2 + 3\tan(\theta)^2}. \tag{2}$$

Since the $[\bar{1}10]$ direction is contained in all surfaces in this family, the intersection of the two planes, (111) and (111) remain in the surface along the [110] direction.

If we assume that dislocations form in all four of these glide planes, then we would expect to find a triangular pattern of intersecting misfit dislocations in a lattice mismatched heteroepitaxial thin film grown above the critical thickness on this family of off-axis substrates. Then, as θ approaches zero the two arrays of dislocations which are oriented at angle φ with respect to each other will align and become indistinguishable from the [110] direction returning to the familiar cross-hatch pattern.

Until recently, this does not seem to have been observed experimentally. Kightley and co-workers[20] found this type of dislocation network in InGaAs grown on off-axis GaAs substrates. The substrates in their experiments were (001) tilted off-axis toward (010) by ∼2°. Since the substrates in their experiments had tilt components in both the [110] and $[\bar{1}10]$, the splitting of the dislocation lines occurred in both directions. They found a separation of ∼2.5° for the dislocation network in both the [110] and $[\bar{1}10]$ surface directions. This loosely corresponds with Eq. (2) which gives a value of ∼1.8°. To our knowledge this phenomenon has not been systematically studied in SiGe systems, and moreover has not been confirmed for large angles. In this paper, we will show that these dislocations appear along directions as predicted by Eq. (2) for heteroepitaxial SiGe films deposited on off-axis substrates with large θ.

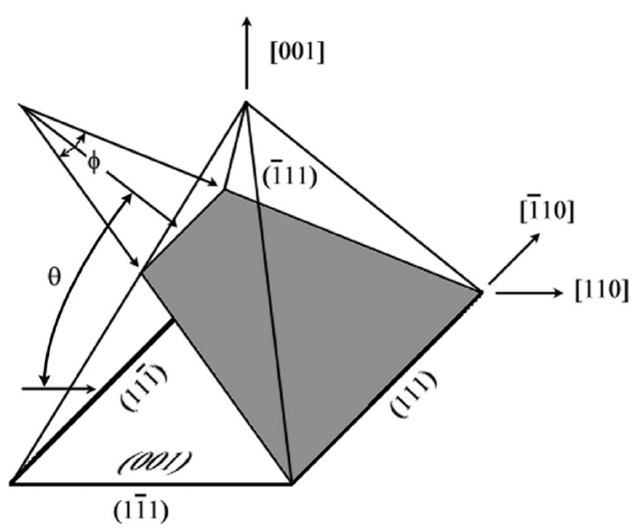

FIG. 1. Diagram of (111) planes intersecting the off-axis surfaces indicated by the shaded region. This demonstrates how the intersection of the (111) and (111) glide planes with the substrate no longer occurs along parallel lines but along lines separated by an angle φ as the substrate is rotated off of the [001] axis about the [110] direction by an angle θ. Similarly, the (111) and (111) planes are no longer both inclined to the substrate at the same angle.

II. EXPERIMENT

Commercially prepared Si substrates were obtained from Virginia Semiconductor, Fredericksburg, Virginia, USA with surface orientations specified off axis from (001) to (111) by 0°, 10°, and 22°. The 0° off-axis samples were nominally (001) substrates. The 10° and 22° substrates were inspected by indexing the plan-view electron diffraction pattern in the transmission electron microscopy (TEM) and to within a degree found to be (116) and (113) surfaces, respectively. We will label these two surfaces as 13° and 25° off of the (001) axis throughout the rest of this article. The substrates were subjected to a wet chemical clean for approximately 60 s using a 10:1 hydrofluoric acid solution diluted in deionized water. Following loading into the UHV system with base pressures in the 10^{-10} Torr range, the substrates were submitted to a thermal treatment at 950 °C for 10 min to desorb any residual contaminants. After cooling to 550 °C, and immediately prior to deposition of the experimental layer, a 20 nm Si buffer layer was deposited. Auger electron spectroscopy (AES) and low-energy electron diffraction (LEED) were used on a sacrificial substrate after deposition of the buffer layer to confirm that the preparation techniques were sufficient. The AES showed only Si within its sensitivity, and the LEED showed a sharp $(2\times1)+(1\times2)$ reconstruction on the (001) substrates. The tilted surfaces showed sharp LEED patterns as well indicating atomically clean surfaces.

Immediately following the buffer layer deposition, the heteroepitaxial layers were formed by codepositing Si and Ge in a UHV solid-source molecular-beam epitaxy at 550 °C at a combined rate of 0.04 nm/s. Layers of $Si_{1-x}Ge_x$, $x=0.3$, were grown to 100 nm on each of the three differently oriented substrates. The deposition is controlled and monitored with dual 6 MHz gold-coated quartz oscillators which have been calibrated by profilometry.

Samples for plan-view TEM were thinned by chemically etching from the back side of the sample until it became electron transparent. The TEM was performed using a JEOL 2000FX microscope operated at 200 kV. All samples were imaged in dark field along the [001] zone axis for dislocation analysis.

III. RESULTS

Shown in Fig. 2 is a plan-view TEM image displaying the two orthogonal misfit dislocation arrays that form for SiGe growth on on-axis (001) Si. This is the familiar pattern of dislocations reported often for this surface.[14]

Plan-view TEM images for the 13° and 25° substrates are shown in Figs. 3 and 4, respectively. Noticeably, the dislocations in the surface [110] directions, i.e., vertical in the plane of the paper, have separated and now intersect at an angle, φ, which increases with the off-axis angle, θ. This pattern of dislocations is diagrammed in Fig. 5 along with that for the (001) surface for reference. All of our samples have been grown above the critical thickness for relaxation of $Si_{0.7}Ge_{0.3}$ on Si (001).[21] Therefore, we expect dislocations, but we have found through Raman measurements that these SiGe films are only about 60% relaxed.[8]

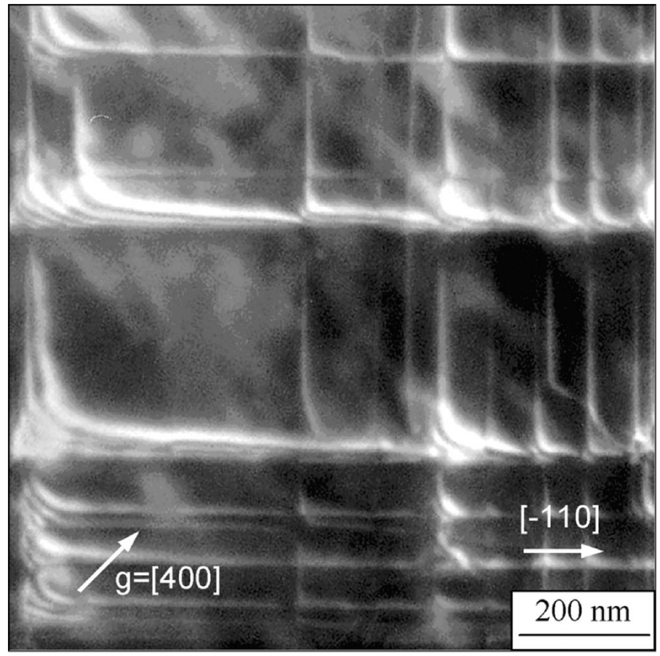

FIG. 2. Plan-view dark-field TEM of 100 nm $Si_{0.7}Ge_{0.3}$ on (001) Si showing orthogonal arrays of misfit dislocations. The curved features at the dislocation intersections are moiré fringes due to superimposed diffraction from the layer and the substrate.

Figure 6 summarizes the measurements of φ for several locations within each of the TEM images. The separation angle, φ, was obtained from a measurement of the various angles of intersection as described in the caption for Fig. 6. It is evident from the plot that there is a distribution in the measurement of φ.

The three different measurements, as described in Fig. 6, of φ should all produce similar results if the surface orientation is within our studied family. This seems to be the case

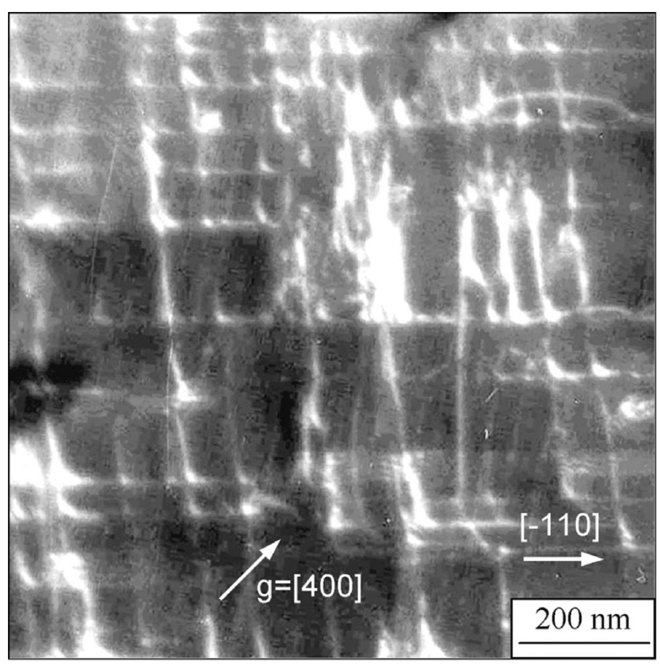

FIG. 3. Plan-view dark-field TEM of 100 nm $Si_{0.7}Ge_{0.3}$ on 13° off-axis Si.

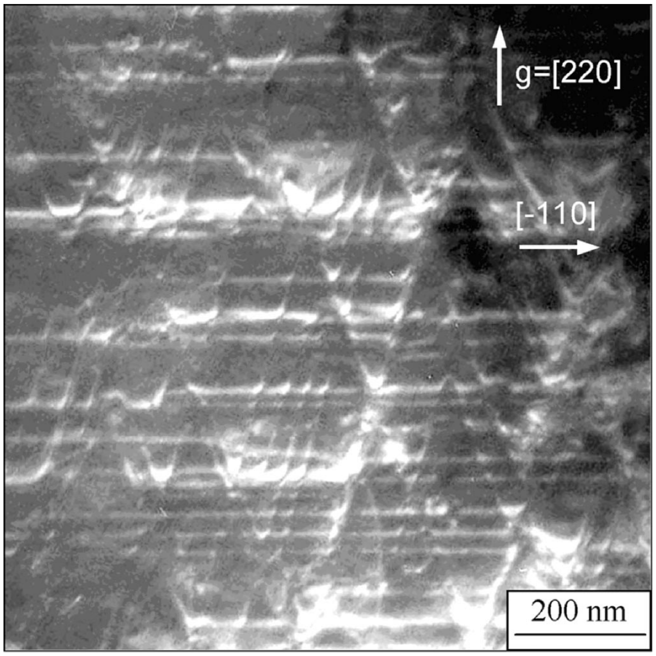

FIG. 4. Plan-view dark-field TEM of 100 nm $Si_{0.7}Ge_{0.3}$ on 25° off-axis Si.

for the 13° off-axis sample with the average of $\varphi=16.8°$ which corresponds to a surface off-axis angle of 12° according to Eq. (2).

The 25° off-axis sample, in contrast, shows three distinct clusters in the distribution of φ around an average value of 34.5° which corresponds to a surface off-axis angle of 26° according to Eq. (2). Each of the clusters within the distribution is the result of determining φ from each of the three angles of dislocation intersection as described in Fig. 6. The discrepancy between the different measurements is attributed to the missorientation between the surface normal and the electron beam in order to achieve the two-beam condition for imaging. This effectively distorts the relevant angles.

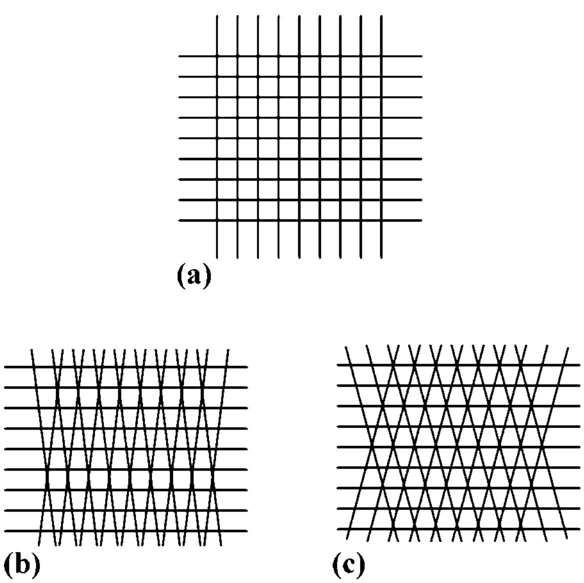

FIG. 5. Diagram showing the predicted configuration of misfit dislocations for (a) on-axis, (b) 13°, and (c) 25° off-axis Si substrates.

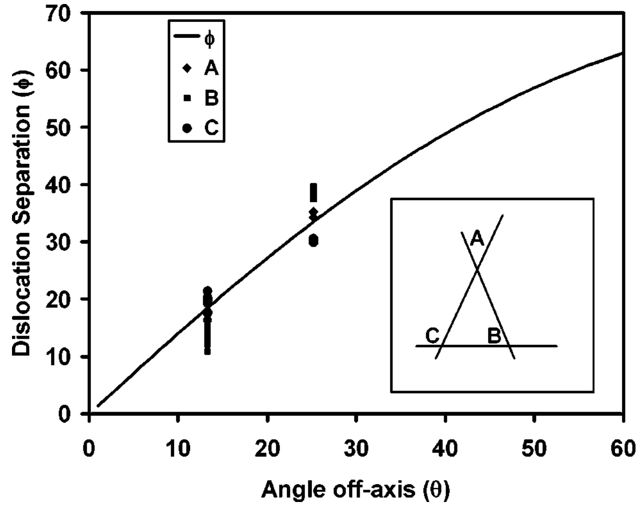

FIG. 6. Plot showing the angular separation of the oblique misfit dislocations. The different measurements: A, B, and C, were found by measuring the angles as diagrammed in the inset. The angle A is the direct measurement of the separation, and B and C are used to find the angle of separation assuming that a line bisecting A is normal to the line BC, i.e., assuming that ABC forms an equilateral triangle. It is immediately evident that the independent measurements of A, B, and C are different, especially for the 25° sample. This is because of the misorientation between the surface normal and electron-beam direction that arises when the sample is tilted into a two-beam diffraction condition. The line labeled φ is a plot of Eq. (2).

IV. DISCUSSION

Dislocation arrays which form in the on-axis samples have been analyzed by others and have been found to be formed by a complex combination of kinetic effects,[19,22] which can be influenced by the morphology of the growth surface.[23] These dislocations with Burger's vector given by $\mathbf{b}=(a/2)\langle 110\rangle$ with a being the lattice constant, are the so-called 60° type where the angle between $\mathbf{b}$ and the line direction of the dislocation is 60°.[16] Misfit dislocations, such as these, relax the misfit strain by an effective amount given by $b^*\cos(\lambda)$, where b is the absolute magnitude of the Burger's vector, $\mathbf{b}$, and λ is the angle between $\mathbf{b}$ and the direction in the interface perpendicular to the dislocation line direction.[24]

Before describing the dislocations in the off-axis samples, we should completely list the possibilities for stable dislocations in the (001) sample. Referring to Fig. 1 in what follows, consider a dislocation lying in the [110] direction in the (111) plane on a (001) interface. There are four minimum lattice translation vectors for the diamond lattice in this case which are the possible Burger's vectors. They are: $\mathbf{b}=(a/2)[110]$, $(a/2)[110]$, $(a/2)[101]$, or $(a/2)[011]$. Of these, only the last two both experience a resolved lattice mismatch stress and can glide in this system. The first of the four is pure screw but experiences no resolved lattice mismatch stress. The second of the four is pure edge type with $\lambda=0°$, thus, it may provide a maximum amount of relaxation if it were to form, but cannot move by glide.[16] So, it is expected that dislocations with $\mathbf{b}=(a/2)[101]$ or $(a/2)\times[011]$, both with $\lambda=60°$, will form in (001) samples for the [110] dislocations in the (111) glide plane. Similar results hold for the other three {111} planes shown in Fig. 1 for the (001) surface.

In general, there is no reason to expect that the dislocations in the SiGe/Si(100) system would consist of any type other than the $(a/2)\langle 110\rangle$ type. But, as the substrate surface is rotated off of the [001] axis, the various $(a/2)\langle 110\rangle$ Burger's vectors contribute differently to the relaxation of misfit strain. Effectively, the angle λ is no longer the same for all dislocation directions. As θ grows, two of the glide planes, (111) and (111), each have unique λ's which we will label $\lambda_{(111)}$ and $\lambda_{(\overline{111})}$. The (111) has the same effective geometry as the (111) plane in the system, and does not need to be treated separately. We will consider the (111) plane which has three λ's which become unique as θ increases. We label two with subscripts a and b, representing the two directions of Burger's vectors which could form on the on-axis substrate. The third is the Burger's vector which would have formed a screw dislocation on the on-axis substrate, i.e., $\mathbf{b}=(a/2)[110]$ and will be labeled with the subscript c. We include the c-type here, since this dislocation gains edge character as the substrate is rotated off axis. The results for calculating $\cos(\lambda)$ for each of these cases assuming the off-axis surface is the $(11m)$ surface are derived in the Appendix and summarized here as follows:

$$
\begin{aligned}
\cos\lambda_{(111)} &= \frac{m-2}{2\sqrt{m^2+2}}, \\
\cos\lambda_{(\overline{111})} &= \frac{m+2}{2\sqrt{m^2+2}}, \\
\cos\lambda_{a} &= \frac{m(m-1)}{2\sqrt{(m^2+2)(m^2+3)}}, \\
\cos\lambda_{b} &= \frac{m(m+1)}{2\sqrt{(m^2+2)(m^2+3)}}, \\
\cos\lambda_{c} &= \frac{2m}{2\sqrt{(m^2+2)(m^2+3)}},
\end{aligned}
\tag{3}
$$

where m is given by

$$
m=\frac{\sqrt{2}}{\tan\theta}. \tag{4}
$$

A plot showing the effective Burger's vector lengths in the plane of the interface, given by

$$
b_{\mathrm{eff}}=|\mathbf{b}||\cos\lambda|, \tag{5}
$$

is shown in Fig. 7. Here the magnitude of the vector $\mathbf{b}$ is given as $a/\sqrt{2}$, where the lattice constant, a, is that of the film as determined by Vegard's law. This b_{eff} is essentially the amount of strain that will be relaxed by the formation of a dislocation in the interfacial plane with the given Burger's vector.

Figure 7 describes how the interfacial projection of the allowed Burger's vectors for each array of dislocations changes as the substrate is rotated. Each dislocation would be expected to have the Burger's vector that will allow for the most strain relaxation. Therefore, we will see the dislocations form with different Burger's vectors as the substrate is rotated. The array of dislocations which form in the $[\overline{1}10]$ directions will all adopt the (111) glide plane, since the Burgers vector for this dislocation provides the largest b_{eff} throughout the entire range of θ. For the oblique array of dislocations, we find a change in $\mathbf{b}$ as the surface passes through the (111) orientation. For these arrays, what would have been a screw dislocation on the (001) surface would then be the dominant dislocation providing relaxation in the interface. Also, we see that for the (111) glide plane, the $(a/2)[011]$ Burger's vector dominates for $\theta<54.7$, i.e., $m>1$, and for the (111) glide plane the $(a/2)[101]$ is the dominant dislocation.

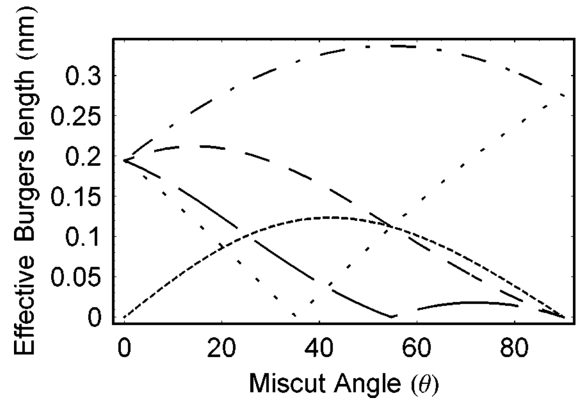

FIG. 7. Plot showing the effective length, from Eq. (5) for the various Burger's vectors involved in the relaxation of off-axis SiGe on Si. The long, medium, and short dashed curves are the Burger's vectors in the [101], [011] and [110] directions, respectively, for the (111) glide plane. Similarly, the long, medium, and short dashed curves represent the [011], [101], and [110] directions, respectively, for the (111) glide plane. The dashed–dotted and the dotted curves are the allowable Burger's vectors in the (111) and the (111) glide planes, respectively.

In a fully relaxed interface, we would expect to find an array of dislocations with some regular spacing. We define the following:

$$
\begin{aligned}
f &= \frac{a_o-a_s}{a_s}=\frac{a_{\mathrm{Si}}(1-x)+a_{\mathrm{Ge}}x-a_{\mathrm{Si}}}{a_{Si}}=\frac{(a_{\mathrm{Ge}}-a_{\mathrm{Si}})x}{a_{\mathrm{Si}}}, \\
p &= \frac{b_{\mathrm{eff}}}{f}, \\
\text{density} &= 1/p,
\end{aligned}
\tag{6}
$$

where f is defined as the fractional misfit. Using lattice constants, $a_{\mathrm{Si}}=0.543\,\mathrm{nm}$ and $a_{\mathrm{Ge}}=0.566\,\mathrm{nm}$, we have, $a_o=a_{\mathrm{Si}}(1-x)+a_{\mathrm{Ge}}x$ for the overlayer with a semi-infinite substrate of lattice constant, $a_s=a_{\mathrm{Si}}$, we can determine the dislocation spacing, p, for a layer that is 100% relaxed due to dislocations with b_{eff} given by Eq. (5). Then, the linear density of dislocations would be given by $1/p$. Table II summarizes the results of this calculation and compares it to data obtained by counting dislocations in a single array in the TEM images. In general, we find that only a fraction of the strain is relaxed by the dislocations in each sample. A simple comparison shows 11% relaxation for the (001) sample, 23% and 28% for the oblique and [110] directions, respectively, on the 13° sample, and 32% and 46% for the oblique and

TABLE II. Calculated for $x=0.3$ [from Eq. (6)] and measured linear dislocation densities for the samples in this experiment. The maximum calculated densities in the first two columns are taken as the density due to the allowed Burger's vector that will provide the most relaxation for that dislocation array. The measured data were taken along a direction perpendicular to each array, and excluding dislocations from other arrays. All directions within each respective sample showed similar densities.

	Maximum oblique density (μm^{-1})	Maximum $[1\bar{1}0]$ density (μm^{-1})	Measured density (from TEM) (μm^{-1})
$\theta=0°$	65.4	65.4	7.0
$\theta=13°$	59.9	50.4	14.0
$\theta=25°$	62.6	43.4	20.0

$[110]$ directions, respectively, on the 25° sample. Raman measurements have shown that these samples are all between 55% and 60% relaxed,[8] so there is a considerable amount of relaxation that is not accounted for by the dislocation densities. Floro *et al.*[25] demonstrated greater than 50% relaxation due to morphological changes in certain dislocation free SiGe films grown on (001) Si. The samples in our study exhibit large corrugations in atomic force microscopy images,[8] which should account for most of the relaxation not mediated by dislocations.

V. CONCLUSION

This study has investigated heteroepitaxial growth of SiGe on a family of Si surfaces that has only recently begun to be fully explored, i.e., those surfaces are between (001) and (111). We have found that the plastic relaxation of the stress is facilitated by misfit dislocations which follow the lines of intersection of the (111) planes with the respective surfaces. This produces a tiled triangular pattern of dislocations at the interface which should continuously vary from equilateral triangles for a (111) surface to the well known cross hatch of dislocations which form for a (001) surface. Generalizing to surfaces in between these limited families, e.g., surfaces of the form $(mn1)$, with $-1\leqslant m,\ n\leqslant 1$, we would expect to find the dislocations which make up the bases of the triangles found in our study split into two intersecting dislocations as the two {111} planes that made up those dislocations become nondegenerate in the plane of the surface. These generalizations, after logically extending them to the $(mn0)$ surfaces, with $-\infty\leqslant m,\ n\leqslant 1\infty$, define the plastic relaxation for strain relaxation on every crystallographic orientation of Si.

ACKNOWLEDGMENT

This work was supported in part by the NSF under Grant No. DMR 0102652. Two of the authors (J.L.G. and R.H.) acknowledge support by NSF-DMR (Grant No. 0075116) under the UVA-UIUC-IBM-Sandia Focused Research Group ''Nanoscale Morphological Evolution of Semiconductor Surfaces.''

TABLE III. The three allowable Burger's vectors for each {111} glide plane intersecting the (001) surface. Note that a factor of $a/2$ has been left off each vector.

Glide plane	(111)	$(\bar{1}\bar{1}1)$	$(\bar{1}11)$	$(1\bar{1}1)$
$\mathbf{b}_1$	$[\bar{1}01]$	$[101]$	$[101]$	$[\bar{1}01]$
$\mathbf{b}_2$	$[0\bar{1}1]$	$[011]$	$[0\bar{1}1]$	$[011]$
$\mathbf{b}_3$	$[\bar{1}10]$	$[\bar{1}10]$	$[110]$	$[110]$

APPENDIX: CALCULATION OF THE COMPONENT OF THE BURGERS VECTORS IN THE PLANE OF THE OFF-AXIS SUBSTRATES

We determine the cofactor used to calculate the amount of relaxation that a dislocation with Burger's vector, **b**, will produce on an interface between surfaces with normals of the form $(11m)$ with $0\leqslant m<\infty$ in the diamond cubic lattice.

We begin by discussing misfit dislocation relaxation in thin-film deposition on the (001) surface. We limit the discussion to the so-called 60° type dislocations which are written as

$$\mathbf{b}=\frac{a}{2}\langle 110\rangle, \tag{7}$$

where a is the lattice constant. The allowed **b**'s are required to be in the glide plane of the dislocation. In Table III, possible Burger's vectors are listed for each of the {111} glide planes which are involved. Note that in each case, $\mathbf{b}_3$ is the screw dislocation allowable on each respective glide plane for the (001) interface. These dislocations remain screw type for the (111) and $(\bar{1}\bar{1}1)$ planes as the surface is rotated off axis, but for the remaining two {111} planes the $\mathbf{b}_3$ Burger's vectors gain edge character, which give them a driving force to form in those systems.

Next, we need to define several vectors. These are not conceptually necessary on the (001) surface as the labeling of the Burger's vector as 60° type tells us all we need to know about that dislocation but, as we move off axis, they will be required. They are as follows:

$$\begin{aligned}
&\mathbf{n}\equiv\text{surface normal},\\
&\mathbf{g}\equiv\text{glide plane normal},\\
&\mathbf{u}\equiv\text{dislocation direction},\\
&\boldsymbol{\xi}=\mathbf{u}\times\mathbf{n}\equiv\text{normal to }\mathbf{u}\text{ in the interface},\\
&\mathbf{b}\equiv\text{Burger's vector}.
\end{aligned} \tag{8}$$

Now, we will define the cofactor by writing the component of the Burger's vector which lies in the interface plane normal to the dislocation, i.e., that part which acts to relax the stress. This is the effective Burger's vector magnitude, or

$$b_{\text{eff}}=|\mathbf{b}||\cos\lambda|, \tag{9}$$

where λ is the angle between **b** and $\boldsymbol{\xi}$. The $\cos(\lambda)$ is the part we will need to calculate for the off-axis substrates. Here, taking the absolute value removes any ambiguity in choosing signs on the vectors in Eq. (8).

For the (001) surface, we know from Eq. (7) that the magnitude of $\mathbf{b}$ is $a/\sqrt{2}$. And, it is well known that λ is 60° for this surface, thus we have

$$b_{\text{eff}}(\{001\}) = \frac{1}{2}\frac{a}{\sqrt{2}}. \tag{10}$$

But, we can calculate cos(λ) by taking the dot product of $\mathbf{b}$ and $\boldsymbol{\xi}$. Since all four glide planes are identical here, we can choose the $(1\bar{1}1)$ plane with Burger's vector, $(a/2)[10\bar{1}]$. In this case, $\mathbf{u}=[110]$ and $\mathbf{n}=[001]$, thus $\boldsymbol{\xi}=[1\bar{1}0]$. Thus, we determine that cos(λ)=1/2.

Rotating the substrate toward the [110] direction by some angle, θ, we can write that $\mathbf{n}=[11m]$, where m need not be an integer in general. By taking the dot product of this $\mathbf{n}$ with [001], we can determine that

$$m = \frac{\sqrt{2}}{\tan\theta}. \tag{11}$$

On these surfaces, now, we no longer have all four glide planes acting equally, so they will need to be treated individually. The (111) and $(\overline{111})$ planes still intersect the surface along the same line, so their associated $\mathbf{u}$'s will not change and can be written as

$$\mathbf{u}_{(111)} = [\bar{1}10],$$

and

$$\mathbf{u}_{(\overline{111})} = [\bar{1}10]. \tag{12}$$

The dislocation directions for the other two glide planes can be determined as follows. To find the lines of intersection of the $(1\bar{1}1)$ and $(\bar{1}11)$ planes with the $(11m)$ plane, we must solve the following sets of simultaneous equations:

$$(1\bar{1}1) \Rightarrow \begin{cases} x - y + z = 0, \\ x + y + mz = 0, \end{cases}$$
$$(\bar{1}11) \Rightarrow \begin{cases} -x + y + z = 0, \\ x + y + mz = 0. \end{cases} \tag{13}$$

Those solutions result in

$$\mathbf{u}_{(1\bar{1}1)} = \left[\frac{m+1}{2}, \frac{m-1}{2}, -1\right],$$

and

$$\mathbf{u}_{(\bar{1}11)} = \left[\frac{m-1}{2}, \frac{m+1}{2}, -1\right]. \tag{14}$$

Now, we can write down the $\boldsymbol{\xi}$'s for all four dislocation lines using the definition in Eq. (8). Dropping any extra constants as all we need are the directions, we are left with

$$\boldsymbol{\xi}_{(1\bar{1}1)} = [m(m-1)+2, -m(m+1)-2, 2],$$

$$\boldsymbol{\xi}_{(\bar{1}11)} = [m(m+1)+2, -m(m-1)-2, -2],$$

and

$$\boldsymbol{\xi}_{(111)} = \xi_{(\overline{111})} = [mm2]. \tag{15}$$

Now, we will determine λ, or more importantly cos(λ), by taking the dot product of an allowed Burger's vector and the $\boldsymbol{\xi}$ of its associated glide plane. For each of the (111) and $(\overline{111})$ planes, we can choose a single Burger's vector, since the two in each plane are oriented similarly with respect to the interface. For the $(1\bar{1}1)$ and $(\bar{1}11)$ planes, the vectors $\mathbf{b}_1$ and $\mathbf{b}_2$ in each are oriented differently with respect to the interface plane, but the two glide planes are mirror images of each other and thus we can just take $\mathbf{b}_1$ and $\mathbf{b}_2$ from the $(1\bar{1}1)$ plane, for example. Then, we must also include $\mathbf{b}_3$ for the off-axis surfaces as it, again, gains edge character. With this, we can now calculate the following:

$$\cos\lambda_{(111)} = \frac{m-2}{2\sqrt{m^2+2}},$$

$$\cos\lambda_{(\overline{111})} = \frac{m+2}{2\sqrt{m^2+2}},$$

$$\cos\lambda_a = \frac{m(m-1)}{2\sqrt{(m^2+2)(m^2+3)}}, \tag{16}$$

$$\cos\lambda_b = \frac{m(m+1)}{2\sqrt{(m^2+2)(m^2+3)}},$$

$$\cos\lambda_c = \frac{2m}{2\sqrt{(m^2+2)(m^2+3)}},$$

where the a and b subscripts delimitate between the $\mathbf{b}_1$ and $\mathbf{b}_2$ Burger's vectors in each of the $(1\bar{1}1)$ and $(\bar{1}11)$ planes, and the c subscript represents the $\mathbf{b}_3$ Burger's vectors in the $(1\bar{1}1)$ and $(\bar{1}11)$ planes.

Finally, we use Eq. (16) in Eq. (9) with the known magnitude of the complete Burger's vector to determine the effective relaxation due to a misfit dislocation in a film grown on one of this family of off-axis substrates. And, using Eq. (11), we can make this a function of θ, the off-axis angle.

[1] *Properties of Crystalline Silicon*, edited by Robert Hull (INSPEC, London, 1999).
[2] M. Orange, Sci. Am. **285**(3), 26 (2001).
[3] A. A. Baski, S. C. Erwin, and L. J. Whitman, Surf. Sci. **392**, 69 (1997).
[4] H. J. W. Zandvliet, H. B. Elswijk, E. J. van Loenen, and D. Dijkkamp, Phys. Rev. B **45**, 5965 (1992).
[5] S. van Dijken, H. J. W. Zandvliet, and B. Poelsema, Surf. Rev. Lett. **5**, 15 (1998).
[6] L. Lapena, I. Berbezier, B. Gallas, and B. Joyce, Thin Solid Films **336**, 124 (1998).
[7] I. Berbezier, B. Gallas, L. Lapena, J. Fernandez, J. Derrien, and B. Joyce, J. Vac. Sci. Technol. B **16**, 1582 (1998).
[8] Mogan E. Ware, Ph.D. thesis, North Carolina State University, 2002.
[9] W. Ranke, Phys. Rev. B **41**, 5243 (1990).
[10] D. J. Bottomley, H. Omi, and T. Ogino, J. Cryst. Growth **225**, 16 (2001).
[11] H. Omi and T. Ogino, Phys. Rev. B **59**, 7521 (1999).
[12] K. Brunner, J. Zhu, C. Miesner, G. Abstreiter, O. Kienzle, and F. Ernst, Physica E (Amsterdam) **7**, 881 (2000).
[13] J. H. van der Merwe, Crit. Rev. Solid State **17**, 187 (1991).
[14] R. Hull and J. C. Bean, Crit. Rev. Solid State **17**, 507 (1992).
[15] J. W. Matthews, in *Epitaxial Growth Part B*, edited by J. W. Matthews (Academic, New York, 1975), p. 559.
[16] R. Hull, in *Germanium Silicon: Physics and Materials*, Semiconductors and Semimetals, edited by R. Hull and J. C. Bean (Academic Press, New York, 1999), Vol. 56, p. 102.

[17] F. K. LeGoues, Mater. Res. Bull. **21**, 38 (1996).
[18] R. Hull, E. A. Stach, R. Tromp, F. Ross, and M. Reuter, Phys. Status Solidi A **171**, 133 (1999).
[19] E. A. Stach, R. Hull, R. M. Tromp, F. M. Ross, M. C. Reuter, and J. C. Bean, Philos. Mag. A **80**, 2159 (2000).
[20] P. Kightley, P. J. Goodhew, R. R. Bradley, and P. D. Augustus, J. Cryst. Growth **112**, 359 (1991).
[21] R. People and J. C. Bean, Appl. Phys. Lett. **47**, 322 (1985).
[22] B. W. Dodson and J. Y. Tsao, Appl. Phys. Lett. **51**, 1325 (1987).
[23] S. B. Samavedam and E. A. Fitzgerald, J. Appl. Phys. **81**, 3108 (1997).
[24] J. Price Hirth and J. Lothe, *Theory of Dislocations*, 2nd ed. (Kreiger, Malabar, Florida, 1982).
[25] J. A. Floro, E. Chason, L. B. Freund, R. D. Twesten, R. Q. Hwang, and G. A. Lucadamo, Phys. Rev. B **59**, 1990 (1999).